# Dynamics of Bound States of Same-Chirality Spiral Waves

Christian Zemlin[1], Karthik Mukund[1], Vadim Biktashev[2], and Arkady Pertsov[1]

[1]*Department of Pharmacology, SUNY Upstate Medical University, Syracuse, New York 13210*
[2]*Department of Mathematical Sciences, University of Liverpool, Liverpool L69 7ZL, United Kingdom*

## ABSTRACT

We describe the dynamics of bound states of same-chirality spirals in a generic numerical model of an excitable medium. For each bound state, we analyze its tip trajectory patterns and determine its characteristic frequencies. We report two new bound states: for spiral pairs, a state that exhibits alternating cycles of small and large distances between collisions ($A_2$); for triplets, the first example of a meandering bound state ($M_3$). In parameter space, $A_2$ lies in between the previously described oscillating pairs ($O_2$) and master-slave pairs ($MS$). We present numerical evidence that the transition $O_2 \rightarrow A_2$ occurs via a supercritical period-doubling bifurcation, while the transition $A_2 \rightarrow MS$ occurs via a symmetry breaking secondary Hopf bifurcation. A classification of all regimes according to dynamical systems theory exposes the wealth of phenomena exhibited by multiarmed spiral waves.

## I. INTRODUCTION

Spiral waves occur in a variety of physical, chemical, and biological systems. Examples include the Belousov-Zhabotinsky reaction [1,2], electrical ativity in cardiac tissue [3], aggregation of starving slime mold amoeba [4], and catalytic reactions on platinum surfaces [5]. At the same time, analytical and simulation studies have greatly advanced our understanding of spiral wave dynamics [6-10].

Two or more spirals can form bound states, i.e. stable ensembles of spiral arms that interact and remain within a limited distance from each other. They have characteristic features, like their frequency [11,12], and rules of interaction with other bound states [12].

An important example of bound states are multiarmed spiral waves, ensembles of same-chirality spiral waves whose tips are separated by less than a core diameter. They have been observed in chemical media, like the Belousov-Zhabotinsky reaction [11], and in biological media, e.g. *Dictyostelium discoideum* [13], two-dimensional cultured heart tissue [14], the whole rabbit heart [15], and a variety of numerical models of excitable media [16].

The simplest type of same-chirality bound states are oscillating multiarmed spirals ($O_n$) [17]. They are characterized by an $n$-fold rotational symmetry and periodic collisions of their arms. Recently, our group discovered another bound state of two same-chirality spirals in which one spiral rotates around the other (master-slave pairs or *MS)* [18]. This state exhibits no symmetry, and the spiral tips are separated by a distance which can be large compared to the diameter of the core of the spiral. Finally, multiarmed spirals rotating around a common core can persist for considerable time [13]; however, they have been shown analytically to be unstable for several FitzHugh-Nagumo type media [9] and are not included in our discussion.

While many papers have commented on the complex dynamics of bound states [11,12,14], these dynamics have not yet been analyzed. In this paper, we study the dynamics of bound states of same-chirality waves in a generic excitable medium. We report a new stable regime of spiral pairs, in which the spiral arms alternate between larger and smaller separations between collisions ($A_2$). A second new regime we found are triple-armed meandering spirals ($M_3$). We characterize the bifurcations that mark the transitions between bound states. We classify all observed regimes in terms of the theory of dynamical systems with symmetry and determine for each regime the parameter region in which it is stable. Table 1 summarizes the properties of the bound states

| Symbol | Bound State | Isotropy Group | Attractor in Orbit Space | Figure |
|---|---|---|---|---|
| $O_n$ | Oscillating multiarmed spirals with $n$ arms | $Z_n$ | Limit cycle | 1 |
| $A_n$ | Alternating oscillating multiarmed spirals with n arms | $Z_n$ | Limit cycle (double period) | 2 |
| $MS$ | Master-slave pairs | $\{id\}$ | Torus | 3 |
| $M_n$ | Meandering multiarmed spirals with $n$ arms | $\{id\}$ | Torus | 4,5 |

**Table 1**: Bound states of same-chirality spiral waves. Grey background indicates bound states that are described in this paper for the first time.

of same-chirality spiral waves.

## II. METHODS

### Numerical methods

All observations were made in numerical simulations in the widely used Barkley reaction-diffusion model [19] of a generic excitable medium. It consists of an activator variable $u$ and an inhibitor variable $v$, which evolve according to:

$$\partial u/\partial t = (1/\varepsilon)u\,(1-u)[u-(v+b)/a] + \nabla^2 u$$
$$\partial v/\partial t = u - v. \qquad (1)$$

The constant $\varepsilon$ is the ratio of characteristic time scales of the activator and inhibitor variables. The parameters $a$ and $b$ represent the slope of the $u$-nullcline and the excitation threshold. We chose a typical value of $\varepsilon$=0.02 and varied $b$ from 0.15 to 0.3. We set $a$=1.1 unless stated otherwise ($a$ was always between 0.9 and 1.25). All of the regimes we describe can be observed in the parameter region for which single-armed spirals rigidly rotate, so the complexity observed here is truly a consequence of the interaction of the spiral arms.

We solved the model equations on a 320x320 or 640x640 grid using Euler's method with zero flux boundary conditions, $dx$=0.1826 as our space step, and $dt$=0.003 as our time step. The tips of spiral waves were defined to be the pixels satisfying $0.45<u<0.57$ and $0<du/dt<10$. All computations were performed on a 32-node Beowulf cluster.

To create bound states of spiral waves, we used two different methods. In the first method, we initiated two consecutive plane waves, let them advance halfway through our medium. We then reset half of our medium, creating two broken wave fronts. In the second method, we superimposed snapshots of a single-armed spiral in equally spaced phases (we summed the values of each variable over the different snapshots, at each point of the medium). When we initiated bound states of three or more arms, we used the second method.

The stability of a bound state was assumed if it showed no sign of decay after at least 100 spiral rotations.

We defined the center of mass of a configuration as the center of mass of the tips. The minimal and maximal tip distances from the center were determined by automatically detecting the minimal and maximal distances for at least 10 periods and then taking the average.

To determine angular velocities in the tip trajectories ($\omega_1$, $\omega_2$, and $\omega_3$; see definitions in the Results section), we measured the time needed for a large number of rotations (at least 10), and divided the covered angle by that time.

When we ramped $b$ to study the dependence of the system's behavior on excitability, we used the final condition of each value of $b$ as the initial condition for the next value of $b$ and allowed transients to pass for at least 15 spiral rotations after each change in $b$. The boundaries of the regimes in parameter space were established with an accuracy of 0.001 in the value of $b$ for any given $a$.

### Classification of multiarmed spiral waves

A convenient language to describe the qualitative features of dynamic regimes is that of the dynamical systems theory [20]. However, this language cannot be directly applied to reaction-diffusion systems, because these systems have spatial symmetry (they are equivariant with respect to the Euclidean group, i.e. translations, rotations, and reflections). An efficient method to deal with this symmetry is to consider the space of group orbits of the system [21], which do not exhibit spatial symmetry. In this section, we explain this method without any attempt of mathematical rigor.

Consider a dynamical system defined in a phase space $V$ and equivariant with respect to a symmetry group $G$. Any point $v \in V$ may have its own symmetry group $H = H(v) \subset G$ which is called the *isotropy* group of point $v$. The isotropy subgroup is the same for all points of a trajectory. The union of all points with similar isotropy subgroups is called a stratum. The phase space $V$ is a disjoint union of strata. Asymmetric solutions have the trivial isotropy subgroup $\{id\}$, consisting only of the identical transformation. For the system (1), the asymmetric solutions are single-armed spirals or asymmetric multi-armed spirals.

We also consider here $n$-armed spiral waves, which are symmetric with respect to rotation by a multiple of $2\pi/n$. Their isotropy groups are isomorphic to the group $Z_n$. A group orbit is a set of points of $V$ obtained from each other by various elements of $G$. By identifying all points belonging to the same orbit, we reduce the phase space $V$ to the orbit space $V/G$. The part of the $V/G$ corresponding to one stratum has a structure of a manifold, and is called an orbit manifold. Any trajectory in $V$ generates a trajectory in $V/G$. The dynamical system in $V/G$ is called the reduced dynamical system. Its is generic in the sense that its dynamics are devoid of the original symmetry of the problem; so we can expect to find standard types of attractors and bifurcations on that system, unlike the original.

For system (1) and $G$ the Euclidean group, in some cases the reduced dynamical system can be understood as system (1) re-written in a moving frame of reference, say attached to the tip of a spiral [22]. Thus we will sometimes refer to (1) as dynamics in the laboratory frame of reference.

An important technical comment in [23] is that any coordinate on the orbit manifold is a group-invariant function of the phase space of (1), and vice versa, any such function can be used as a coordinate on an orbit manifold unless it is a constant for that manifold.

To summarize, the implications important for our present study are:

• The understanding of the dynamic regimes of multiarmed spiral waves should be in terms of dynamics on the orbit manifolds by the Euclidean group, and this can be achieved by using Euclidean invariant functions of such solutions.

• The structure of the orbit manifold depends on the symmetry (the isotropy subgroup) of the solutions in question, and as long as the solutions in question are within one stratum, i.e. have the same symmetry, the dynamics on the group manifold is generic, in particular, should be expected to demonstrate attractors and bifurcations typical for generic, non-symmetric systems.

Moreover, by Takens' embedding theorem [24], just one such coordinate is almost certainly sufficient to reconstruct qualitatively the dynamic attractor. In our simulations, the symmetry of solutions was always evident, so no special technique for its detection was needed. As the Euclidean-invariant characteristic of two-armed spiral wave solutions we have used the distance $d(t)$ between the two tips, which was easy to measure and interpret. Then we applied to $d(t)$ the standard delayed embedding technique to reconstruct the attractors.

For symmetric three-armed solutions, we used the distance between one of the tips and the center of symmetry as the Euclidean-invariant characteristic, which is also group-invariant and practical inasmuch as the center of symmetry can be found with sufficient accuracy.

## III. DYNAMICS OF THE MULTIARMED SPIRAL REGIMES

### Oscillating pairs ($O_2$)

Figure 1 shows the detailed dynamics of $O_2$. The two spiral tips approach each other (Fig. 1A), collide (Fig. 1B), and move apart again (Fig. 1C). Between collisions, both tips follow a circular trajectory of the same radius an isolated single spiral wave (Fig. 1C-D), until they collide again at their tips (Fig. 1E). The relative positions of the spiral arms at each collision are identical (Fig. 1B, E), but from one collision to the next, both arms are rotated around the center of symmetry. This second rotation explains the petal pattern (Fig 1F) that the tip trajectories form over several rotations. Figure 1G shows the distance between the tips as a function of time. It is strictly periodic with period $T$.

The tip trajectories can thus be described as a combination of a steady rotation of each spiral arm around its core and periodic discrete rotations, at each collision, of the whole pair. To quantify the steady rotation, we define the petal frequency $\omega_1 = 2\pi/T$. The periodic rotation of the whole pair can be interpreted as a second, slower rotation: We name the

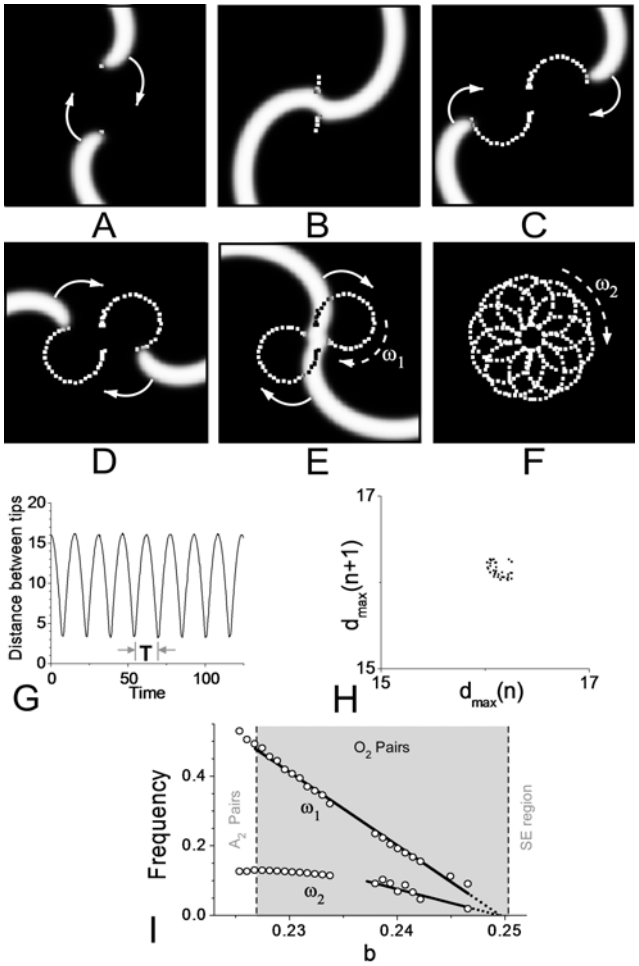


**Figure 1.** Representative example of $O_2$ dynamics ($b$ = 0.2303). Thick white lines show the excitation waves ($u \approx 1$), dotted white lines show the tip trajectories. Arrows indicate the drift direction of the tips. **A-E:** Evolution of $O_2$ over 1.5 periods. **F:** Tip trajectories of $O_2$ over four periods. **G:** The distance $d$ between the tips as a function of time. **H:** Recurrence map for the Poincare cross-section defined by the local maxima of $d(t)$. **I:** Petal frequency $\omega_1$ and meandering frequency $\omega_2$, as a function of $b$. The $O_2$ region is marked grey, the adjacent regimes ($A_2$, $SE$) are discussed below.

angle of deflection $\alpha_2$ and define the meandering frequency $\omega_2 = \alpha_2/T$. After head-on collisions, we always assumed that the tips exchange their spiral arms. The reason for this convention is that for collisions away from the tip, the tips manifestly exchange arms, and with our convention, we treat all collisions equally.

The sign of $\omega_1$ was the same as that of $\omega_2$ in all our simulations, and we set $\omega_1, \omega_2 > 0$ without loss of generality (taking the mirror image of the medium changes the sign of both $\omega_1$ and $\omega_2$). From the definitions of $\omega_1$ and $\omega_2$ it follows immediately that $\omega_1 > \omega_2$. We describe in the Methods section how we measure $\omega_1$ and $\omega_2$.

Figure 1H shows a recurrence map for the Poincare cross-section defined by the local maxima of $d(t)$. Since there is no discernable structure in the recurrence map and the changes in the maxima of $d(t)$ are minimal, we conclude that the

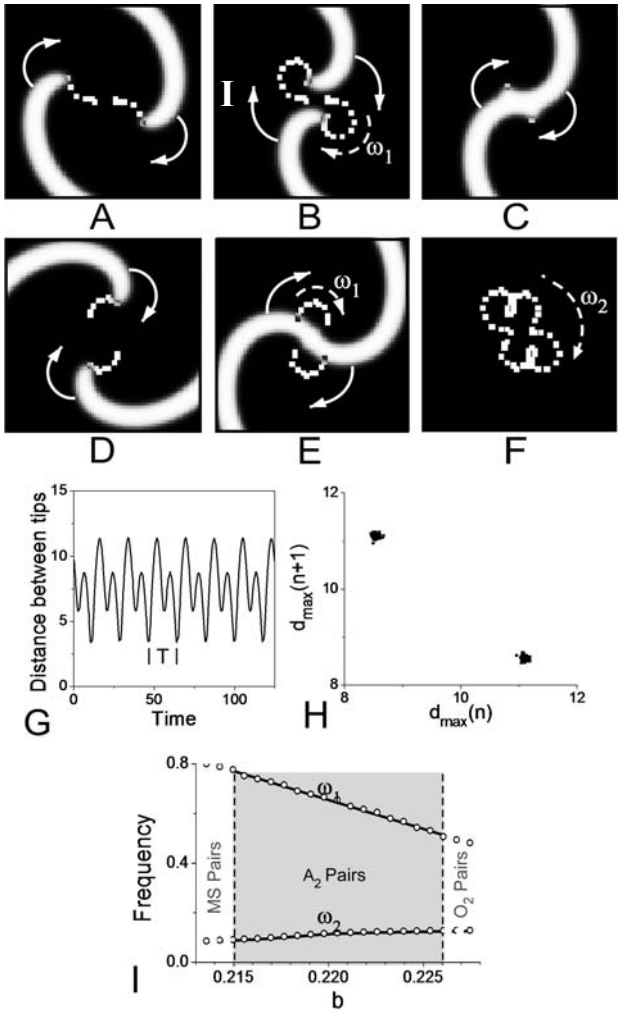


**Figure 2.** Representative example of $A_2$ dynamics ($b$ = 0.2177). **A-E:** Evolution of $A_2$ over one period. **F:** Tip trajectories of $A_2$ over one period. **G:** The distance $d$ between the tips as a function of time. **H:** Recurrence map for the Poincare cross-section defined by the local maxima of $d(t)$. **I:** Petal frequency $\omega_1$ and meandering frequency $\omega_2$ as a function of $b$. The $A_2$ region is marked gray, the adjacent *MS* regime is discussed below.

attractor of $O_2$ in orbit space is a limit cycle, i.e. we have a periodic solution of the reduced system. In the laboratory frame of reference, this generates a bi-periodic solution. This is similar to the classical flower-pattern meander of single-armed spirals, only here both tips describe the same flower patterns symmetrically.

Figure 1I shows $\omega_1$ and $\omega_2$ as a function of $b$. The dependency of $\omega_1$ on $b$ is in good approximation linear. Extrapolating the $b$ for which $\omega_1$ is 0 leads to good agreement with the largest $b$ that supports spiral pairs (as well as single spirals). This should be expected, because the single spiral radius grows to infinity as we approach the boundary of the spiral pair domain, and consequently $\omega_1$ should vanish. Our extrapolation of $\omega_2$ reaches zero at practically the same value of $b$; this can also be expected because $\omega_1 > \omega_2$ (see above).

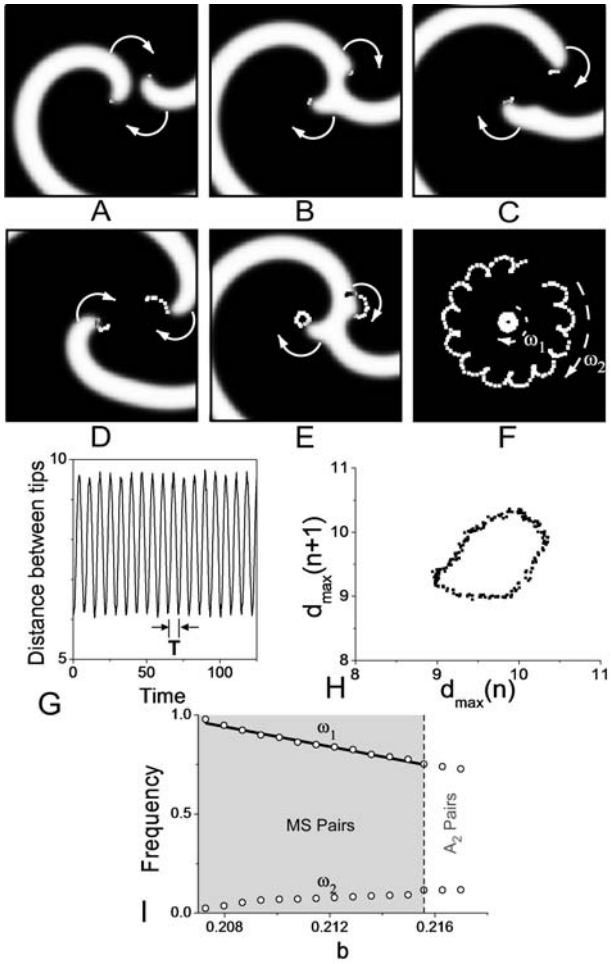


**Figure 3.** Representative example of *MS* dynamics ($b$ = 0.2087). **A-E:** Evolution of *MS* over one period. **F:** Master and slave tip patterns for one complete revolution of the slave around the master. **G:** The distance $d$ between the tips as a function time. **H:** Recurrence map for the Poincare cross-section defined by the local maxima of $d(t)$. For this panel, we used $b$=0.2214 (see text). **I:** Petal frequency $\omega_1$ and meandering frequency $\omega_2$ as a function of $b$.

As $b$ is decreased, $\omega_2$ grows, but the growth saturates towards the end of the $O_2$ regime.

The observed $O_2$ regime corresponds to the stable spiral pairs described by Ermakova et al. for a different FitzHugh-Nagumo medium [17].

### Alternating pairs ($A_2$)

Figure 2 shows a new, alternating regime of spiral pairs, which we call $A_2$. As in the case of $O_2$, the two spiral arms maintain perfect center ($Z_2$ -) symmetry (Figs. 2A-E). However, $A_2$ exhibits two different types of collisions that occur alternatingly. The first type of collision is "sideways": The initial contact between the two arms occurs at some distance from the tip (Fig. 2C). The second type is "head-on", i. e. collision occurs close to the tip (Fig. 2E), as for $O_2$. Figure 2F shows that the tip trajectories in the two types of

inter-collision periods also differ: They form a petal pattern that contains two different petal sizes.

Figure 2G shows the distance between the tips as a function of time, where alternans can also clearly be seen. Figure 2H shows the recurrence map for the Poincare section defined by the local maxima of $d(t)$.

The empirical attractor consists of two clusters, neither of which has any further discernible structure. We conclude that the attractor in orbit space of $A_2$ is a limit cycle; but this time, the period is about twice that of an isolated spiral in the same medium.

Figure 2I shows that the linear increase of $\omega_1$ with decreasing $b$ continues throughout the $A_2$ domain, while $\omega_2$ begins to decrease. Note that for $A_2$, the period $T$ between collisions is alternating (say, between $T_1$ and $T_2$). Thus, our definitions of $\omega_1$ and $\omega_2$ need to be modified to $\omega_1 = 4\pi/(T_1+T_2)$ and $\omega_2 = \alpha_2'/(T_1+T_2)$, where $\alpha_2'$ is the angle that the whole pair rotates during the time $T_1+T_2$.

From the formal viewpoint, the orbit space dynamics here are periodic, as for $O_2$, although the shape of the oscillations is more complicated. We will discuss the relationship between $A_2$ and $O_2$ orbit space dynamics in more detail below.

### Master-slave pairs (*MS*)

Figure 3 shows a third regime of double-armed spiral waves (*MS*), in which the central symmetry is broken. The spiral tip that is to the left in Fig. 3A rotates apparently unaffected by the collisions through the entire sequence shown in Figs. 3A-E. At the same time, the other tip is annihilated in every collision (Figs. 3B, 3E) but develops again afterwards (Fig. 3C) We call the spiral that belongs to the unaffected tip "master" and the other spiral "slave". The master takes over the slave arm after each collision, and the slave re-develops from the truncated master arm. Panel F shows master and slave tip trajectories. The distance between master and slave, averaged over one collision period, converges to its steady state within a few revolutions of the slave around the master.

Figure 3G shows that the distance between the tips is in a good approximation periodic, but that the extrema vary slightly from beat to beat.

This variation is further analyzed in Fig. 3H, which shows the recurrence map for the Poincare section defined by the local maxima of $d(t)$. The recurrence map forms a closed loop, and we conclude that the attractor in orbit space of *MS* is a torus. In the Figure, we show the recurrence map for $b$=0.2214, because the loop is more pronounced for larger $b$, for which master and slave are close together (Fig. 3I suggests that $b$=0.2214 does not support *MS*, but there is actually *MS*/$A_2$ bistability for $b$=0.2214, as we discuss below, in Fig. 9).

In Fig. 3I, we see that $\omega_1$ continues to grow as $b$ decreases. On the contrary, $\omega_2$ approaches zero as we approach the left end of the *MS* domain. This is because the master-slave distance diverges towards the left end of the *MS* domain while the petal size (like the radius of an isolated spiral) decreases.

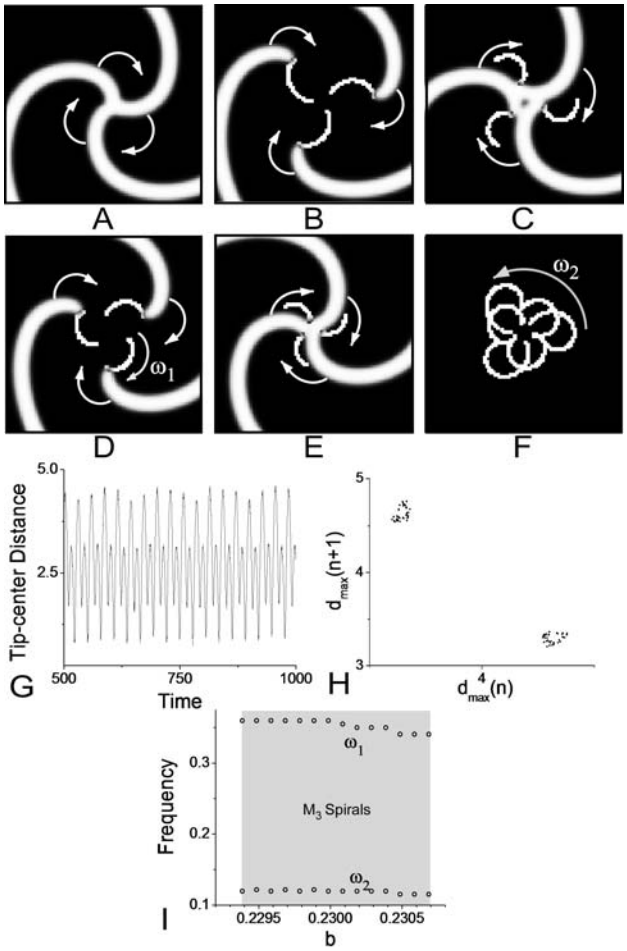


**Figure 4.** Representative example of $M_3$ dynamics (a = 1.25, b = 0.27488). **A-E:** Evolution of stable triple-armed spirals over two periods. We observed two types of collisions, which alternate every rotation cycle: head-on collisions (Frames A, E), and sidearm collisions (Frame C). **F:** Tip trajectory of a triple-armed spiral over two periods. The alternating tip and sidearm collisions form two concentric patterns. **G:** Distance $d$ from the tips to the center as a function of time (equal for all three arms). **H:** Recurrence map for the Poincare cross-section defined by the local maxima of $d(t)$. **I:** Petal frequency $\omega_1$ and meandering frequency $\omega_2$ as a function of $b$.

### Meandering triplets ($M_3$)

We now turn to spirals with three arms. Figure 4 shows the dynamics of a triple-armed, meandering spiral wave ($M_3$). Apart from its meandering, the configuration is analogous to $A_2$: Between collisions, the individual tips move along circular trajectories, as independent single arms. There are two types of collisions that occur alternatingly: head-on (Fig. 4A, 4E) and sideways (Fig. 4C). The tip trajectories also form a pattern analogous to that of alternating spiral pairs, characterized by a small petal radius and a big petal radius (Fig 4F).

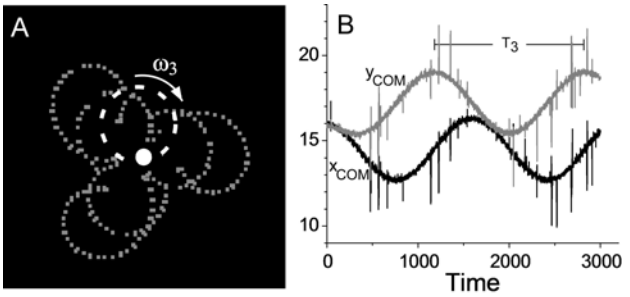


**Figure 5.** Representative example of a meandering multiarmed spiral ($a$=1.2, $b$=0.262). **A:** Tip trajectories and meandering. The dotted gray lines mark the tip trajectories of all three tips, the solid white dot marks the corresponding center of mass of the tips. Over time, the center of mass moves along the circle marked by a dashed white line, with angular velocity $\omega_3$. **B:** Coordinates of the center of mass as a function of time. The black trace shows the $x$-coordinate of the center of mass ($x_{COM}$), the grey trace the $y$-coordinate ($y_{COM}$). Noise in both traces is due to tip misdetections.

Figure 4G shows the tip distance over time, reflecting the alternating motion. Figure 4H shows the recurrence map for the Poincare section defined by the local maxima of $d(t)$. The recurrence map shows two closed loops, so it provides evidence that the attractor in orbit space of $M_3$ is a torus.

However, the structure of the loops is not clear enough to rule out a more complicated attractor, e.g. a 3-torus, which is suggested by the observation of meander discussed below.

Figure 4I shows the petal frequency ($\omega_1$) and the meandering frequency ($\omega_2$) as a function of $b$. Both $\omega_1$ and $\omega_2$ remain almost constant over the $A_3$ domain (which is relatively small).

Figure 5A shows that the whole triplet meanders on a circular path. The amplitude of the meandering is comparable to the core diameter of an isolated spiral. We define the angular meandering velocity $\omega_3=2\pi/T_3$, where $T_3$ is the period of the meandering (see Fig. 5B). The frequency $\omega_3$ depends on $b$ (like $\omega_1$ and $\omega_2$), and it is consistently lower than $\omega_2$ by an order of magnitude (we have not determined the detailed dependency of $\omega_3$ on $b$ because of the very long duration of the corresponding simulations). Figure 5B shows the $x$- and $y$-coordinates of the center of mass ($x_{COM}$ and $y_{COM}$) for a representative example of $M_3$. Despite some noise from tip misdetections, Fig. 5B shows that both coordinates oscillate sinusoidally with great accuracy.

Different from the previously discussed regimes, $M_3$ was stable only for a narrow range of parameters and initial conditions. In the vicinity of this narrow range, $M_3$ can persist for a long time (>50 rotations) before developing asymmetries and finally decaying. This raises the possibility that $M_3$ is nowhere truly stable, but only has very large decay times for certain parameters. While we cannot rule out this possibility, we ran simulations with up to 500 spiral rotations without seeing any sign of breakup. Even if $M_3$ should not be analytically stable, it persists for so long that it can be considered stable for many practical purposes.

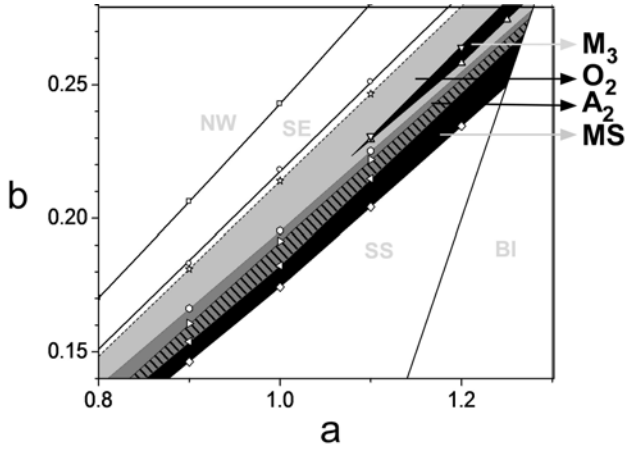


**Figure 6.** Parameter regions of the dynamic regimes of the Barkley model. Light grey area marks the $O_2$ regime, medium grey area the $A_2$ domain, and black area the $MS$ domain. The hatched area marks the overlap of the $A_2$ and the $MS$ domain. Previously identified regimes are labeled in grey: NW (no waves), SE (sub-excitable), SS (stable spirals), and BI (bistable).

### Parameter regions of the dynamic regimes

Figure 6 shows the parameter regions of all dynamical regimes discussed in this paper. They all lie inside the region in which a single spiral is stable (marked "SS"). $O_2$ occurs at highest $b$ (lowest excitabilities), $A_2$ at lower $b$, and $MS$ at still lower $b$. Figure 6 shows that stable bound pairs cover a large portion of parameter space, i.e. more than 50% of the stable spiral (SS) domain shown in Fig. 6 (but note that the SS domain extends beyond the part of the model's parameter space shown in Fig. 6 [25]). The domain of symmetric triple armed spirals is much smaller (about 2% of the SS domain shown in Fig. 6).

We also looked for stable bound states with four arms, but they consistently broke up after a short time (10 rotations). Stable bound pairs also occurred for parameters outside the range shown in Fig. 6 (e.g. for $a$=0.6, $b$=0.08). We never observed them, however, for parameters at which a single spiral meanders [25].

## IV. TRANSITIONS BETWEEN THE REGIMES

### Transition $O_2 \rightarrow A_2$

Figure 7 shows the transition from $O_2$ to $A_2$. Figure 7A shows that starting from the largest value shown ($b$=0.234), decreasing $b$ decreases $r_1$ (maximal distances of the spiral tips from the center of symmetry, see Fig. 7B) and increases $r_2$ (minimal distances of the spiral tips from the center of symmetry, right before a collision, see Fig. 7B). The decrease in $r_1$ reflects the decrease of a single spiral's radius with $b$, and the growth in $r_2$ indicates that the spirals are meeting less and less exactly head-on.

At $b_{O2\rightarrow A2} \approx 0.229$, a period doubling bifurcation occurs in the base system. For $b < b_{O2\rightarrow A2}$, during one period, $r$ does not simply oscillate between $r_1$ and $r_2$, but it increases from $r_2$

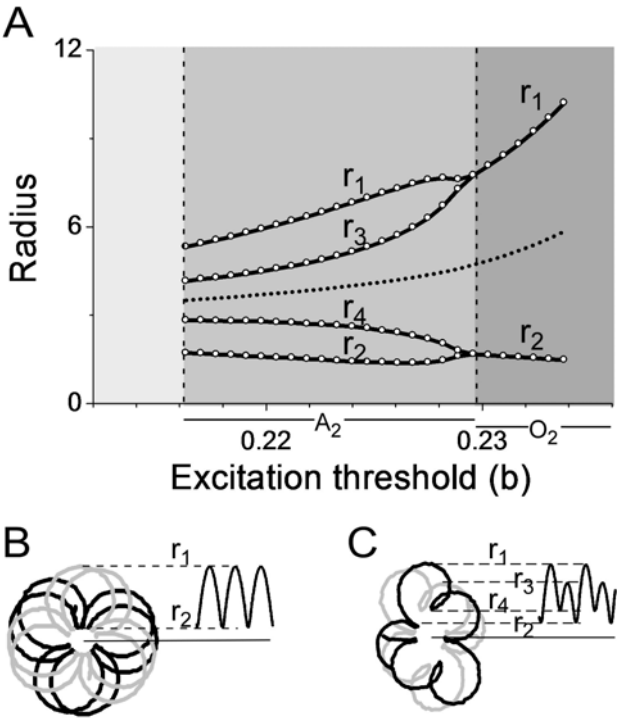


**Figure 7.** Transition from $O_2$ to $A_2$ as $b$ is changed ($a$=1.1). **A:** Bifurcation diagram. The symbols $r_1$, $r_2$, $r_3$, and $r_4$ correspond to the extremal points of the tip trajectories (see Panels B and C). The dark grey area marks the range of $b$ supporting $O_2$, the medium grey area the range of $b$ supporting $A_2$. The light grey area marks the region of $b$ that supports *MS* but not $A_2$ (see Fig.8) . The dotted line indicates the average distance of the spiral tips from the center of symmetry. **B:** Tip trajectories of both spiral arms (grey and black) for $O_2$. Maximum and minimum distances between tips and the center of symmetry are labeled $r_1$ and $r_2$. **C:** Tip trajectories for $A_2$. Additional local maxima and minima are labeled $r_3$ and $r_4$.

to $r_1$, then decreases to $r_4$, increases to $r_3$ and decreases back to $r_2$ (see Fig. 7C). The average radius $[r_1+ r_2+ r_3+ r_4]/4$, shown by a dotted line in Fig. 7A, decreases monotonically down to the end of the alternating pairs domain ($b_{A2\to MS}$≈0.216).

Figure 8 gives evidence that the transition $O_2\to A_2$ is indeed a period doubling bifurcation. Figure 8A shows the delay-embedded distance between the tips for $b$=0.233, i.e. in the $O_2$ domain but close to $b_{O2\to A2}$. The trajectory is a closed loop. Figure 8B shows the corresponding trajectory for $b$=0.226, in the $A_2$ domain. The closed loop has split in a double loop, but the shape is still very similar to that of Fig. 8A. This strongly suggests that a period-doubling bifurcation occurred.

### Transition $A_2\to MS$

Figure 9 shows the transition from $A_2$ to *MS*. In order to characterize the change in *MS* dynamics for different $b$, we introduce the slave precession radius $r_s$ and the master precession radius $r_m$ (Fig. 9B). Figure 9A shows that as $b$ is decreased below $b_{MS\to A2}$≈0.223, the medium begins to sustain *MS* (the name $b_{MS\to A2}$ will become clear in the next paragraph

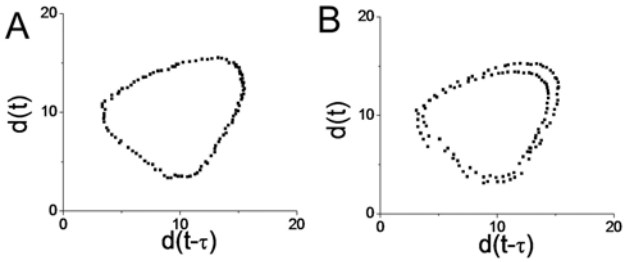


**Figure 8:** Delay-embedded trajectories before (Panel A, $b$=0.233) and after (Panel B, $b$=0.226) the period doubling bifurcation. The delay τ was chosen to be $T$/4 ($T$ measured before the bifurcation).

where we discuss hysteresis). The values of $r_s$ and $r_m$ are on either side of the corresponding average tip-center distance of the $A_2$ regime (dotted line). While $r_s$ grows monotonically and eventually diverges at $b$=0.2057, $r_m$ decreases monotonically and approaches zero as $r_s$ diverges [18].

Note that there is an overlap of the $A_2$ and the *MS* domains. In the bistable region, the initial condition determines whether $A_2$ or *MS* develops. If $b$ is varied continuously, there is hysteresis: Starting with $A_2$ and decreasing $b$ slowly, the alternating pair persists down to $b_{A2\to MS}$≈0.216, while starting with *MS* and increasing $b$ slowly, *MS* persists up to $b_{MS\to A2}$≈0.223.

Below $b_{A2\to MS}$, *MS* is the only stable formation. For decreasing $b$, the slave precession radius increases and eventually diverges around $b$=0.2057 [18] while the master precession radius converges to zero.

Note that the transition from $A_2$ to *MS* is a transition from a limit cycle to an invariant torus in the reduced system. Recall that such a transition is a typical codimension one event in generic dynamical systems, marked by a secondary Hopf bifurcation, a.k.a. Neimark-Sacker bifurcation. In our case this is a symmetry-breaking bifurcation, as different branches correspond to different strata: $A_2$ has central symmetry $Z_2$, whereas *MS* has the trivial symmetry $\{id\}$. Besides, this bifurcation appears subcritical, which gives rise to the 'hard' birth of the 2-torus and the hysteresis.

## V. ROBUSTNESS OF MULTIARMED SPIRAL REGIMES

We performed additional simulations to demonstrate that the regimes described are robust against noise and perturbations and independent of initial conditions.

Figure 10 illustrates the reversibility of the effect of parameter changes. Figure 10A shows the tip trajectories for a value of $b$ that corresponds to $O_2$. Then $b$ is abruptly increased such that the spiral pair remains in the $O_2$ regime, but the resulting tip trajectory pattern has a smaller radius (Fig. 10B). Afterwards, we set $b$ back to its original value and get the original tip trajectory, up to a shift and a rotation (Fig. 10C).

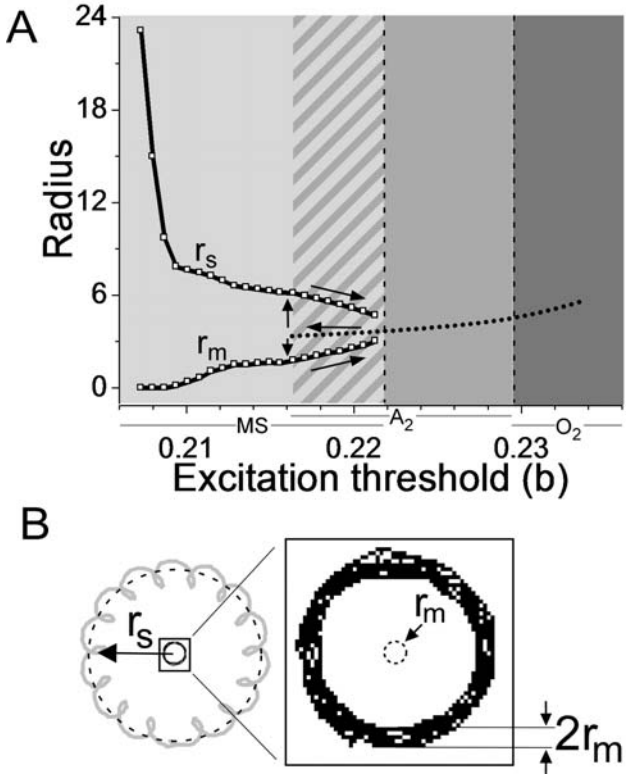


**Figure 9.** Transition from $A_2$ to *MS* as $b$ is changed ($a$=1.1). **A:** Bifurcation diagram for $r$ as $b$ is changed. The symbols used are explained in Panels B and C. The solid lines show $r_s$ and $r_m$ as function of $b$. The dotted line indicates the average distance of the spiral tips from the center of symmetry (copied from Fig.7). Arrows indicate which stable branch the system follows for increasing and decreasing $b$. There is hysteresis in the transition. The dark grey area marks the range of $b$ supporting $O_2$, the medium grey area the range of $b$ supporting $A_2$, and the light grey area the region of $b$ that supports *MS*; note the overlap of the *MS* and $A_2$ domains (hatched area). **B:** Precession of the slave and master. Left panel shows the tip trajectories of slave (grey) and master (black). The motion of the slave tip is a combination of a single spiral rotation and a low-frequency precession of amplitude $r_s$ caused by the interaction. The dashed circle marks the precession component of the trajectory. The trajectory can be recovered by moving the core center along the dashed circle as the tip rotates around the core. In the right panel, we show the magnified master tip trajectory, which appears thick because the motion of the master tip is also a combination of a single spiral rotation and a low-frequency precession of (low) amplitude $r_m$. The dashed circle in the center of the master tip trajectory (radius $r_m$) shows the precession component of the master trajectory. The thickness of the slave trajectory is $2r_m$ because this is how much the instantaneous center of the master rotation changes due to precession.

Transitions between different pairs of regimes are reversible in the same manner. Figures 10D-F illustrate this finding in the case of the regimes *MS* and $O_2$ Figure 10D shows a *MS* tip trajectory. When we abruptly increase $b$, the system converges to the $O_2$ tip trajectory pattern shown in Fig. 10E. When we set $b$ back to its original value, the system evolves back to the *MS* regime and the original tip pattern (Fig. 10F).

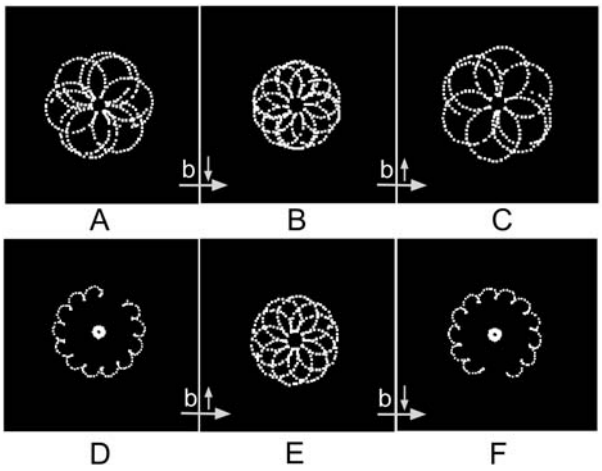


**Figure 10.** Reversibility of the effect of parameter changes. **A-C:** Parameter changes within a dynamic regime ($O_2$). **A:** $O_2$ tip trajectory ($b$ = 0.2338). **B:** Steady-state tip trajectory of the same spiral pair after $b$ is decreased to 0.2303. **C:** After $b$ is decreased to its original value, the original tip pattern is restored. **D-F.** Parameter changes across regimes. **D:** *MS* tip trajectory ($b$ = 0.2149). **E:** Increasing the value of $b$ to 0.2303, we obtain $O_2$. **F:** After decreasing the value of $b$ back to 0.2149, the original $O_2$ is restored.

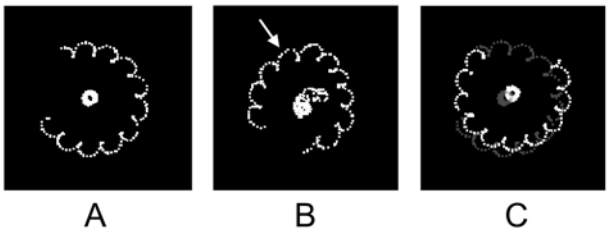


**Figure 11.** Effect of random noise on *MS*. **A**: Tip trajectories of master and slave before noise was switched on. **B:** Transition from noise-free to noise *MS* dynamics. The arrow marks the position in the slave trajectory where the noise was turned on. The master trajectory deviates visibly from its original circular path as soon as the noise is switched on. **C:** Tip trajectories after the noise has been turned off. In the background (grey) we show the original trajectories from Panel A (notice the shift of the entire trajectory pattern). The noise applied consisted of uniformly distributed random numbers with amplitude of ±7.5% of the activation threshold, added in every time step.

We conducted further tests of the robustness of all reported regimes. Figure 11 shows the effect of noise on *MS*. Figure 11A shows the tip trajectories of a master-slave pair before noise is switched on. In Fig. 11B, the noise is off initially, but it is switched on when the slave tip is at the point indicated by the arrow. As soon as the noise is turned on, the slave trajectory becomes irregular; but qualitatively, the *MS* dynamics are preserved. The master trajectory is also affected: As soon as the noise is switched on, the master tip starts to meander randomly on top of its circulating motion. In Figure 11C, the noise has been turned off again, and a regular *MS* tip pattern sets in immediately. We show in grey the original *MS* tip pattern (from Fig. 11A), and see that the

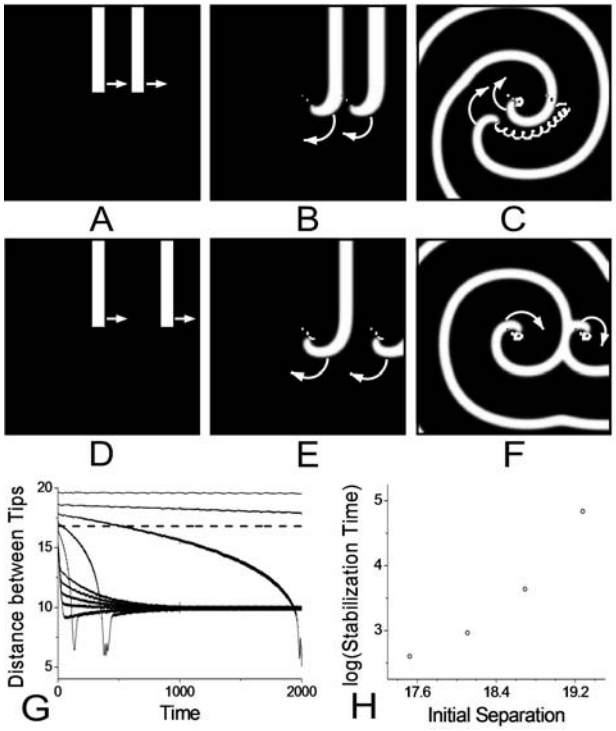


**Figure 12.** Initiation of *MS* from two closely spaced wave breaks. **A-C:** If the distance between the wavebreaks is below some critical value, they develop into *MS*. **D-F:** If the wavebreaks are too widely spaced, they develop into two independent spirals. **G:** Evolution of tip distance for different initial distances. The dashed line marks the single spiral wavelength. **H:** Time for *MS* formation as function of initial separation of the wavefronts.

only lasting effect of the noise application is a small shift of the entire tip trajectory pattern.

We found that the steady state to which the system evolves is generally not sensitive to the initial conditions (exceptions to this rule are discussed below). Initiating any of the reported regimes in two different ways (see Methods section) resulted in an identical steady state (up to a shift and a rotation). Ramping the parameter $b$ led to the same result. Triple-armed spirals did not develop from a train of three consecutive broken waves.

We further applied one-time global additive perturbations of varying amplitude and spatial frequency to the activator variable. These perturbations did not destroy the regimes' dynamics and had a negligible effect on their phase, even for perturbation amplitudes of 0.9 activation thresholds (No figure shown).

The size of the medium and boundary conditions were relevant only if one of the tips got close to the boundary (when the distance became less than the core diameter of an isolated spiral).

While the steady state is generally not sensitive to initial conditions, there are some exceptions. One example is the bistability shown in Fig. 7; in this part of parameter space, some initial conditions lead to $A_2$ and others to *MS*. Another example is shown in Fig. 12: *MS* will develop from a pair of wavebreaks only if they are sufficiently close together (Fig. 12A-C), but not if their separation is above a certain threshold (Fig. 12D-F).

Figure 12G shows the evolution of the tip distance for different initial separations. For initial separations below a threshold $\theta$ ($\theta \approx 15$), the tip distance relaxed monotonously to that of a *MS* pair, $d_{MS}$ ($d_{MS} \approx 10$). For initial separations larger than $\theta$, we observe qualitatively different dynamics: The tip distance first drops below $d_{MS}$ ("undershoot"), and then relaxes to $d_{MS}$. Interestingly, the relaxation to *MS* occurs faster for an initial separation that lies slightly above $\theta$ than for one that lies slightly below $\theta$. However, as the initial separation is further increased, the formation time for a *MS* pair grows dramatically. Figure 12H shows how the formation time of a *MS* pair depends on the initial separation in a semi-logarithmic plot. Formation was considered to occur when the tip distance enters the interval $d_{MS} \pm 5\%$ and stays in this interval. The data points deviate upwards from a straight line; therefore, the formation time either grows super-exponentially or there is some threshold separation above which the two spiral arms do not interact.

## VI. DISCUSSION

In a generic numerical model of an excitable medium, we found two new alternating bound states ($A_2$ and $M_3$) of spiral waves. We observed for the first time meandering in multiarmed spirals ($M_3$). We showed the detailed dynamics of $A_2$, $M_3$, and the two other types of bound states that occur in this model ($O_2$ and *MS*). We scanned the entire parameter space and determined the domains of $A_2$, $O_2$, and *MS*. Each domain occupies a significant portion of parameter space.

We have presented numerical evidence that the transition $O_2 \rightarrow A_2$ occurs via a supercritical period-doubling bifurcation in the reduced system, while the transitions $A_2 \rightarrow MS$ occurs via a symmetry breaking secondary Hopf bifurcation in the reduced system, from the $Z_2$ stratum to the $\{id\}$ stratum. The $O_2 \rightarrow A_2$ period doubling bifurcation is supercritical, thus the birth of the alternating spirals is 'soft'. On the contrary, the $A_2 \rightarrow MS$ secondary Hopf-bifurcation is subcritical, thus the small 2-tori are born unstable, the transition to the new regime is 'hard', and there is hysteresis.

While we analyzed the prevalence of bound states in the whole parameter space, our analysis was limited to states that exhibit strict synchronization of the arms. There are other regimes in our model as well as in other models that lack such synchronization [12,16]. The detailed dynamics of these regimes have not yet been studied and are likely to be more complex.

Our simulations were naturally limited in time, and the regimes that persisted in our simulations may not be analytically stable but decay at a later time. This possibility seems most likely in the case of $M_3$ which was stable in our

simulations only in a narrow range of parameters and initial conditions. In any case, the bound states presented here persist over very long periods and can be considered stable for many practical purposes.

Experimental data on multiarmed spirals exhibit a striking overall resemblance with our numerical simulations. In the Belousov-Zhabotinsky reaction, double- and triple-armed spirals have been observed to periodically move apart and back together [11], much like our double-armed (Figs.1-3) and triple-armed (Fig. 4-5) spirals. Unfortunately, available experimental data do not yet include detailed tip trajectories or bifurcation analyses, and we do not know whether the regimes and transitions we described here occur in experimental systems as well.

Our data suggest, however, that at least some of the bound states we described and the transitions between can be observed in experiments. On the one hand, most of them occupy a significant portion of parameter space, on the other hand, they are robust against various types of perturbations. The chances may be particularly good in media whose experimental parameters can be controlled, as the Belousov-Zhabotinsky reaction. In this reaction, the excitation threshold is perfectly controllable and multiarmed spirals have already been observed [11].

## ACKNOWLEDGEMENTS

Research in this article has been supported by AHA grant #0325458T, by NIH grants 5P01HL039707, 5R01HL071635, and 5R01HL071762, by NSF Grant CTS-0319555, and by EPSRC grant EP/D500338/1(UK). We thank Rebecca Smith and Arvydas Matiukas for carefully reading the manuscript.

---

[1 ] A. N. Zaikin and A. M. Zhabotinsky, Nature **255**, 535 (1970).
[2 ] A. T. Winfree, Science **175**, 634 (1972).
[3 ] J. M. Davidenko *et al.*, Nature **355**, 349 (1992).
[4 ] K. J. Lee, E. C. Cox, and R. E. Goldstein, Phys. Rev. Lett. **76**, 1174 (1996).
[5 ] M. Bär, I. G. Kevrekidis, H. H. Rotermund, and G. Ertl, Physical Review E **52**, R5739-R5742 (1995).
[6 ] V. Zykov, *Simulation of Wave Processes in Excitable Media* (Manchester University Press, Manchester, 1984).
[7 ] A. Mikhailov , *Foundations of Synergetics I*, 2nd ed. (Springer, 1994).
[8 ] A. V. Panfilov and A. V. Holden, *The Computational Biology of the Heart* (Wiley, Chichester, 1997).
[9 ] V. Hakim and A. Karma, Phys Rev E **60**, 5073 (1999).
[10 ] F. H. Fenton, E. M. Cherry, H. M. Hastings, and S. J. Evans, Chaos **12**, 852 (2002).
[11 ] K. I. Agladze and V. I. Krinsky, Nature **296**, 424 (1982).
[12 ] R. M. Zaritski and A. M. Pertsov, Phys Rev E **66**, 066120 (2002).
[13 ] B. Vasiev, F. Siegert, and C. Weijer, Phys Rev Lett **78**, 2489 (1997).
[14 ] N. Bursac, F. Aguel, and L. Tung, Proc Natl Acad Sci U S A **101**, 15530 (2004).
[15 ] T. J. Wu, M. A. Bray, C. T. Ting, and S. F. Lin, J Cardiovasc Electrophysiol **13**, 414 (2002).
[16 ] R. Zaritski , J. Ju, and I. Ashkenazi, Int J Bifurcation and Chaos **15**, (in press).
[17 ] E. A. Ermakova, A. M. Pertsov, and E. E. Shnol, Physica D **40**, 185 (1989).
[18 ] Zemlin C.W. *et al.*, Phys Rev Lett **95**, 098302 (2005).
[19 ] D. Barkley, M. Kness, and L. S. Tuckerman, Phys. Rev. A **42**, 2489 (1990).
[20 ] Y. A. Kuznetsov, *Elements of Applied Bifurcation Theory*, 2nd ed. (Springer, New York, 1998).
[21 ] V.S. Afraimovich , V.I. Arnold , Y.W. Il'yashenko , and L. P. Shilnikov, *Dynamical Systems-5* (Springer, Berlin, 1984)
[22 ] V. N. Biktashev , A. V. Holden , and E. V. Nikolaev, Int J Bifurcation and Chaos **6**, 2433 (1996).
[23 ] P. Chossat, Acta Applicandae Mathematicae **70**, 71 (2002).
[24 ] F. Takens, *Dynamical Systems and Turbulence* (Warwick, 1980)
[25 ] S. Alonso, F. Sagues, and A. S. Mikhailov, Science **299**, 1722 (2003).